Atomic rearrangements in amorphous Al_20_3 under electron-beam irradiation

doi: 10.1063/1.4790705

Atomic rearrangements in amorphous Al_2O_3 under electron-beam irradiation

R. Nakamura,[1,a)] M. Ishimaru,[2] H. Yasuda,[3] and H. Nakajima[2]
[1]*Department of Materials Science, Graduate School of Engineering, Osaka Prefecture University, Gakuen-cho 1-1, Naka-ku, Sakai 599-8531, Japan*
[2]*The Institute of Scientific and Industrial Research, Osaka University, Mihogaoka 8-1, Ibaraki, Osaka 567-0047, Japan*
[3]*Research Center for Ultra-High Voltage Electron Microscopy, Osaka University, Mihogaoka 7-1, Ibaraki, Osaka 567-0047, Japan*

(Received 1 October 2012; accepted 22 January 2013; published online 13 February 2013)

The electron-irradiation-induced crystallization of amorphous Al_2O_3 (a-Al_2O_3) was investigated by *in-situ* transmission electron microscopy under the wide electron-energy region of 25–300 keV. The formation of γ-Al_2O_3 nanocrystallites was induced by irradiating the a-Al_2O_3 thin film along with the formation of nanovoids in the crystalline grains regardless of the acceleration voltage. The crystallization became more pronounced with decreasing the electron energy, indicating that electronic excitation processes play a dominant role in the formation of γ-Al_2O_3. Radial distribution analyses suggested that a-Al_2O_3 transforms to γ-phase via the "excited" ("stimulated") amorphous state, in which the breaking and rearrangement of unstable short-range Al-O bonds, i.e., fivefold-coordinated Al-O (AlO_5) basic units, occur. © *2013 American Institute of Physics*. [http://dx.doi.org/10.1063/1.4790705]

I. INTRODUCTION

Aluminum oxide (alumina, Al_2O_3) is a highly insulating ceramic with great technological applications due to its high melting point, high hardness, low electrical conductivity, and chemical stability. Many different forms, the so-called polytypes, exist in Al_2O_3. α-Al_2O_3 is the most stable corundum form and β-, γ-, η-, and θ-Al_2O_3 are well-known metastable phases.[1] In addition, amorphous Al_2O_3 is of technological and scientific importance as a coating material, which can be obtained through thin film production methods such as evaporation and sputtering, and thermal and anodic oxidation processes on aluminum surface. Among the many types of Al_2O_3, aside from α-Al_2O_3, the structures of amorphous and γ-Al_2O_3 have been studied most extensively, both experimentally and theoretically.[2–4]

Amorphous Al_2O_3 (a-Al_2O_3) is known to transform into γ-Al_2O_3 at elevated temperatures.[1] In our recent studies, it was found that a-Al_2O_3 becomes nanoporous structure as a result of change in amorphous structure and crystallization above 973 K in air.[5–7] The evolution of nanopores can be explained by the self-organization of extra atomic-level spaces in a-Al_2O_3, whose density is about 20% lower than γ-Al_2O_3. The introduction of large amounts of nanopores into γ-Al_2O_3 is expected to be effective in use of γ-Al_2O_3 as catalyst and catalyst support.[8] Therefore, further researches on how to control and/or induce phase transformation at nano to sub-nano scale are required from both the scientific and technological point of view.

Irradiation with energetic particles such as ions, neutrons, and electrons is one of the possible ways for structural control as an alternative to thermal annealing processes. Especially, an electron beam can modify the atomistic structures of a target material without any impurity doping through the mechanisms such as elastic interactions (knock-on mechanism) and excitation-related processes involving breaking or rearrangement of unstable bonds. As for the irradiated effect on polymorphic Al_2O_3, it has been shown extensively for the thermodynamically stable α-Al_2O_3 that intense electron irradiation can produce various defects such as point defects, dislocations,[9–11] planar defects,[12,13] voids,[9,10,14] and aluminum precipitates[12–21] and induce the phase transformation into metastable κ-Al_2O_3.[22] On the contrary, the effect of electron irradiation on the structural change in a-Al_2O_3 still remains unexplored. Although Pan *et al.*[23] and Murray *et al.*[24] reported that nanoparticles and sputter-deposited thin films of a-Al_2O_3 transformed into γ-Al_2O_3 under electron irradiation at 300 and 200 kV, respectively, the mechanisms on structural change, namely, atomic rearrangements, in a-Al_2O_3 during the crystallization into γ-Al_2O_3 under irradiation is far from understood.

Transmission electron microscopy (TEM) is useful for directly observing materials' response under electron-beam-irradiation. In particular, information on progressive structural change from a-Al_2O_3 to γ-Al_2O_3 as a function of irradiation energy and dose can be extracted via radial distribution function (RDF) analysis, by taking electron diffraction patterns from nearly identical region of a specimen. In this study, electron-beam-induced structural changes in an a-Al_2O_3 thin film were investigated by *in-situ* TEM under the acceleration voltages of 25–300 kV.

II. EXPERIMENTAL PROCEDURES

Thin films of a-Al_2O_3 were prepared by an electron-beam (EB) technique in a high-vacuum chamber. High-purity tablet of Al_2O_3 (99.99%) and cleavage NaCl crystal were used as the evaporation source and the substrate, respectively. The substrate at deposition was at ambient temperature. The NaCl on which the 15–20 nm thick oxide thin film was deposited was put into distilled water, and then the floating thin film was mounted onto a Pt grid. Electron-irradiation and observation

[a)]E-mail: nakamura@mtr.osakafu-u.ac.jp.

were carried out using Hitachi H-7000 TEM at 25–125 kV, Hitachi H-800 TEM at 200 kV, and JEOL 3000F TEM at 125–300 kV. The beam current density in the central part of the electron beam was measured using a Faraday cage by placing the electron beam away from the sample. To calibrate the readouts of current and current density from two different machines, the electron intensities were recorded on imaging plate (Eu^{2+}-doped BaFBr) as a function of acceleration voltages and exposure times. The response of the imaging plate is linear to the applied electron dose in a broad dynamic range, and the beam intensities were analyzed quantitatively using an imaging plate processor, specifically a Digital Micro-Luminography FDL 5000 system (Fuji Film). Electron diffraction patterns from an irradiated area were also recorded on an imaging plate for radial distribution function analyses.

III. RESULTS AND DISCUSSION

A. Crystallization mechanisms of a-Al_2O_3

A typical example of the changes in morphology and structure of a-Al_2O_3 associated with electron-irradiation at ambient temperature is shown in Fig. 1. The incident electron-energy and the dose rate were 200 keV and 1×10^{22} e m^{-2} s^{-1}, respectively. No contrast fluctuation can be detected in an as-deposited a-Al_2O_3 film, as shown in the bright field image (BFI) of Fig. 1(a), indicating that no crystalline grains are included in the as-deposited a-Al_2O_3. In fact, halo rings due to the amorphous structure are observed in the selected-area electron diffraction (SAED) pattern of Fig. 1(a). In the as-deposited film, a small amount of voids, which were introduced in the deposition process, were observed in defocused images. After irradiation for 1.8 ks (Fig. 1(b)), crystalline grains with a diameter around 3 nm appear as indicated by the contrast fluctuation. As shown in the SAED patterns in Fig. 1(b), the weak Debye-Scherrer ring corresponding to the (440) plane of γ-Al_2O_3 can be detected. Further irradiation (for 4.5 ks) induces the crystallization into γ-Al_2O_3 as shown in the BFI and SAED of Fig. 1(c). It is noteworthy that void contrast becomes clearer as crystallization proceeds. The crystallization of a-Al_2O_3 into γ-Al_2O_3 through not only thermal annealing above 973 K (Refs. 5 and 7) but also irradiation at ambient temperature is accompanied by void formation.

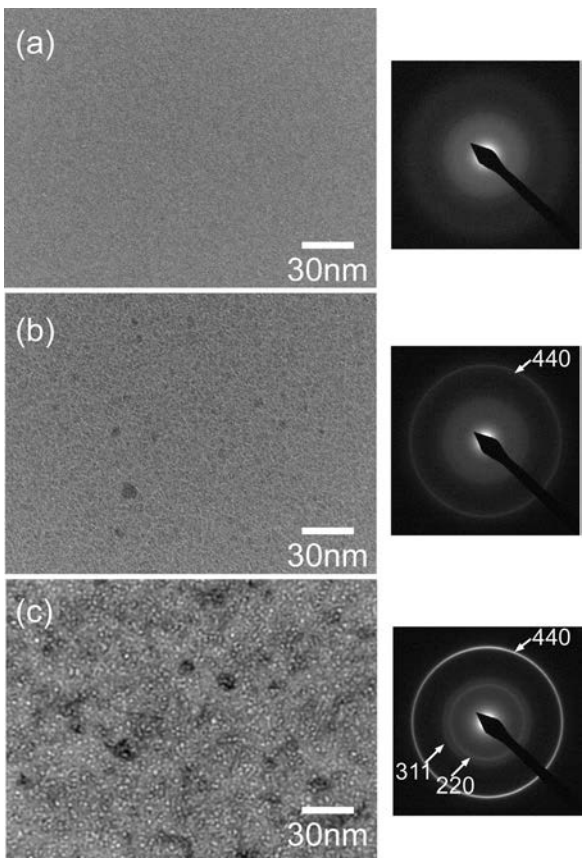

FIG. 1. A typical example of changes in morphology and structure of a-Al_2O_3 induced by electron-irradiation: (a) before irradiation, (b) after irradiation for 1.8 ks, and (c) for 4.5 ks at an acceleration voltage of 200 kV and a dose rate of 1×10^{22} e m^{-2} s^{-1}.

The crystallization of a-Al_2O_3 by a 200-keV electron beam was also observed by Murray *et al.*,[24] who concluded that the crystallization was attributed to temperature rise during irradiation. In fact, γ-Al_2O_3 is formed by thermal annealing of a-Al_2O_3 above 973 K.[5,7] Here, we examined how much temperature rise would occur during irradiation. The highest temperature rise, T, due to beam heating for a uniform film sample can be estimated using the following equations:[25,26]

$$T = W_0[1 + 2\ln(R/r_0)]/4\pi l_0 k; \quad W_0 = \varepsilon V \rho_0 \pi r_0^2, \quad (1)$$

where W_0 is the total absorbed power, R is the radius of the film within a hole of supporting metal grid (here 6.4×10^{-5} m), r_0 is the radius of the irradiated region (here 2×10^{-7} m), l_0 is the specimen thickness (here 1.5×10^{-8} m), k is the thermal conductivity (here 1.6 W m^{-1} K^{-1} for anodic alumina film[27]), ε is the fraction of energy absorbed, usually 0.01,[28] V is the accelerating voltage (here the highest voltage 2×10^5 V), and ρ_0 is the current intensity (here 6×10^2 A m^{-2}). For the present irradiation conditions, the temperature rise in the irradiated area was calculated to be 6 K based on the Eq. (1). Actually, we obtained an experimental evidence that indium (melting temperature: 429 K) nanoparticles on a-Al_2O_3 were kept isolated during irradiation (supplementary figure[29]), indicating that the temperature rise during irradiation is so small that the coalescence of nanoparticles is not induced. Based on both the theoretical and experimental results, we can conclude that the effect of beam heating should be excluded as a contributing factor for crystallization.

To clarify the origin of the crystallization, we examined the irradiation energy dependence of crystallization. Figure 2 shows the SAED patterns taken from the nearly identical region of a-Al_2O_3 films irradiated under the electron energy of (a) 25 and (b) 300 keV at ambient temperature. The dose rate under 25 keV, 2.5×10^{19} e m^{-2} s^{-1}, is 1/20 as small as that under 300 keV, 5.8×10^{20} e m^{-2} s^{-1}. The irradiated region is smaller at 300 keV than 25 keV in order to realize higher dose rate at 300 keV. The crystallization of a-Al_2O_3 takes place along with the preferential appearance of the Debye-Scherrer rings corresponding to the (440) planes of γ-Al_2O_3, as indicated by arrows, regardless of the energy of incident electrons. As shown in Fig. 2(a), the Debye-Scherrer ring for (440)

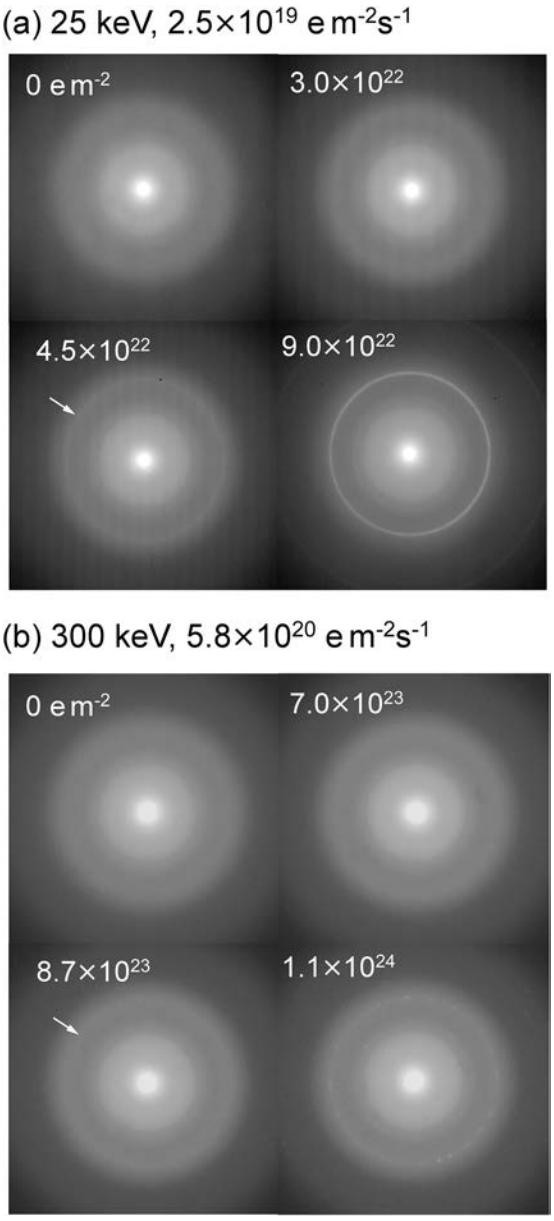

FIG. 2. *In-situ* observation of SAED patterns taken from nearly identical region of irradiated a-Al_2O_3: (a) 25 keV and 2.5×10^{19} e m^{-2} s^{-1} and (b) 300 keV and 5.8×10^{20} e $m^{-2}s^{-1}$. The appearance of the Debye-Scherrer ring corresponding to (440) pattern of γ-Al_2O_3 is indicated by the arrow.

appears clearly after the irradiation of 4.5×10^{22} e m^{-2} although it does vaguely at 3.0×10^{22} e m^{-2}. The dose of irradiated electrons required for inducing crystallization varies according to the energy of incident electrons: 8.7×10^{23} e m^{-2} at 300 keV is 20 times larger than 4.5×10^{22} e m^{-2} at 25 keV. The Debye-Scherrer rings appearing at 25 keV are continuous while those at 300 keV are somewhat discontinuous and some strong reflections exist. This is attributed to the difference in the size of irradiated region; the small number of γ-Al_2O_3 grains contributes to the formation of the diffraction pattern in Fig. 2(b).

Two types of damage processes can occur during electron irradiation: one is elastic displacement and the other is excitation-related processes. Roughly speaking, the former and the latter processes are dominant at higher and lower

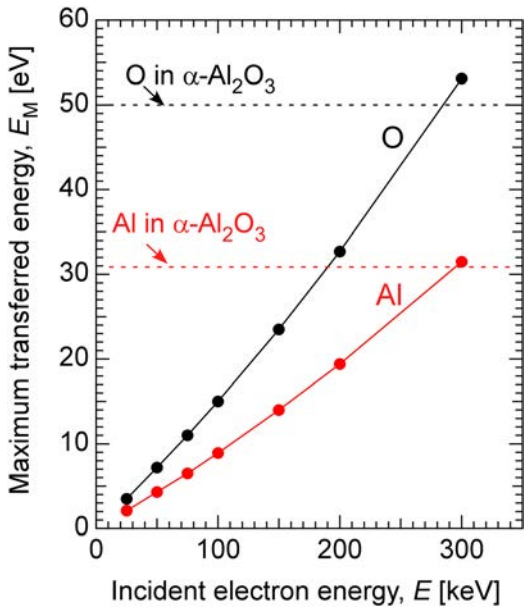

FIG. 3. The relationship between the maximum transferred energy, E_M, for Al and O and an incident electron energy E. The threshold displacement energies for Al and O in α-Al_2O_3 are shown together for reference as broken lines.

electron energy ranges, respectively. The maximum transferred energy, E_M, from an incident electron of mass m_e and kinetic energy E to a constituent atom of mass m_a can be calculated using the following equation:[26,30]

$$E_M = 2m_aE(E + 2m_ec^2)/[(m_a + m_e)^2c^2 + 2m_aE], \quad (2)$$

where c is the velocity of light. The equation is derived from the conservation law of momentum for relativistic electrons. E_M for Al and O calculated from the Eq. (2) is plotted against incident electron energy in Fig. 3. The experimentally collected threshold displacement energies for Al and O in α-Al_2O_3 are known to be 20–32 and 50 eV,[31] respectively, while the literature data on displacement energies in a-Al_2O_3 are unavailable. The upper values for Al (32 eV) and O (50 eV) are shown as dotted line in Fig. 3. The elastic displacement mechanism is likely to be dominant in α-Al_2O_3 above 300 keV since E_M for both Al and O is higher than the upper value of threshold displacement energy at 300 keV. It should be noted that the knock-on energy of the surface atoms is smaller than that of the inside atoms. This means the composition change due to surface sputtering should be considered. Figure 4 shows energy-dispersive X-ray spectra as a function of electron flux, obtained from the nearly identical region of a-Al_2O_3 irradiated at 300 keV. The peak intensity of O-K_α decreases slightly with the increase of electron dose. From the quantitative analysis, it was confirmed that the composition change is insignificant (~2%). In addition, no Bragg reflections due to Al precipitates are observed in the diffraction patterns of Figs. 1 and 2. These results suggest that the crystallization of a-Al_2O_3 is not due to the surface sputtering during irradiation.

As described above, the electron dose for crystallization at 300 keV is much larger than that at 25 keV (Fig. 2). To realize the crystallization dose, the experiments at different

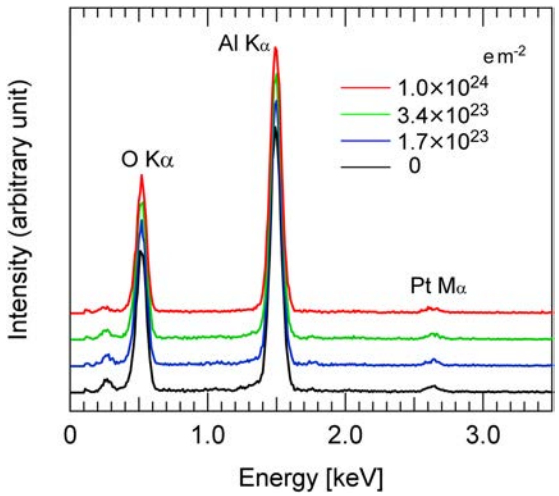

FIG. 4. Energy-dispersive X-ray spectra for a-Al_2O_3 during irradiation at 300 keV. These spectra are normalized by the peak height of Al-K_α.

voltages had different dose rates in the present study. The dose rate is an important factor in irradiation experiments, and therefore, we examined if the crystallization process would be dose-rate independent. In Fig. 5(a), the dose for crystallization, at which the Debye-Scherrer ring corresponding to the (440) plane starts to appear, is plotted against the dose rate. The dose for crystallization is almost constant against dose rate at 125 and 300 keV. This result suggests

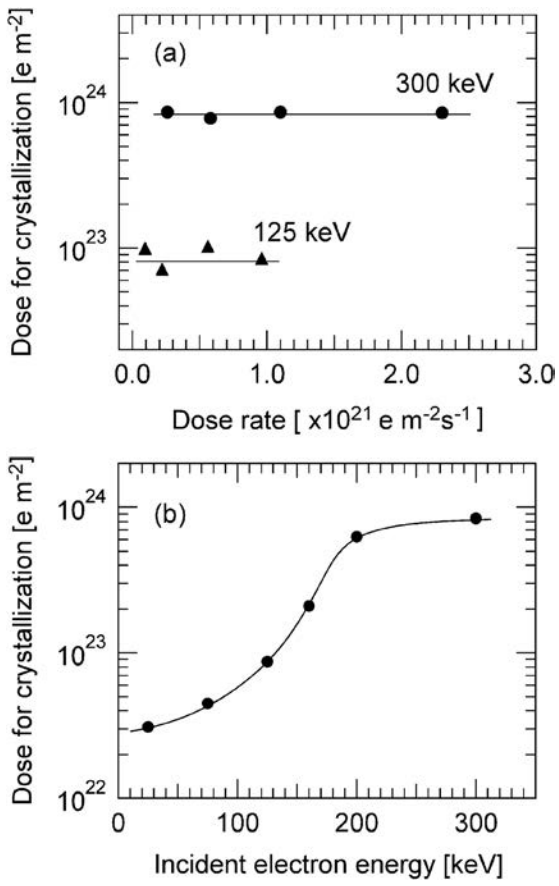

FIG. 5. (a) Dose for crystallization of a-Al_2O_3 into γ-Al_2O_3 plotted against dose rate at 125 and 300 keV. (b) Averaged dose for crystallization as a function of the energy of incident electrons.

that the crystallization mechanisms remain unchanged at constant electron energy under the present irradiation conditions, then allowing us to discuss the electron-energy dependence of crystallization mechanisms. Figure 5(b) shows the dose for crystallization vs incident electron-energy. Each data point shows the average value of 3–5 measurements at different electron fluxes under each electron energy, as shown in Fig. 5(a), and the experimental error (standard deviation) is within $\pm 10\%$ of the average value. The dose required for crystallization is 3×10^{22} e m^{-2} at the lowest incident electron energy of 25 keV and then increases rapidly with increasing electron energy up to 200 keV. Above 200 keV, however, the slope of increase in dose for crystallization is suppressed. The threshold displacement energies in a-Al_2O_3 are expected to be lower than those in the most stable phase of corundum α-Al_2O_3 (20–32 eV for Al and 50 eV for O), and therefore, the saturation of the dose is probably due to the enhancement of the knock-on effects. The energy-dependence of crystallization observed here clearly indicates that electronic excitation during irradiation is a dominant mechanism of the crystallization of a-Al_2O_3. The crystallization via excitation-related processes is also observed in amorphous $ScPO_4$ and $LaPO_4$ by Meldrum *et al.*[32]

B. Atomic rearrangements in electron-irradiated a-Al_2O_3

RDF analysis is one of the useful methods to characterize the amorphous structures of materials. In the case of electron irradiation experiment in a transmission electron microscope, in particular, RDF analysis has an advantage in the *in-situ* observation of sequentially structural change by taking electron diffraction patterns from nearly identical regions of the specimen. As shown in the TEM image of Fig. 1, γ-Al_2O_3 appears in the a-Al_2O_3 matrix with the crystallite size of a few nanometers. This situation makes it possible to obtain continuous Debye-Scherrer rings from the irradiated regions with the diameter of 300 nm (Figs. 1 and 2) thereby giving a further advantage in capturing the sequential change in amorphous structure toward γ-Al_2O_3 by RDF analysis. The detailed procedures of RDF analysis using electron diffraction techniques are described elsewhere.[33,34]

Figure 6 shows the changes in atomic pair distribution functions (PDFs) under irradiation at 100 keV with the dose rate of 4.0×10^{19} e m^{-2} s^{-1} obtained by a quantitative analysis of the SAED patterns. In Fig. 6(a), the PDFs for before and after irradiation under four dose conditions are selectively compared to catch the overall picture of structural change. The intensity-peaks of Al-O, O-O, and Al-Al bonds can be seen at around 0.18, 0.28, and 0.32 nm, respectively, which is in good agreement with a number of experimentally obtained and simulated PDFs of amorphous Al_2O_3.[2,3,6,7,35] After irradiation, remarkable changes are observed in these peaks. The intensity-peaks of O-O, Al-Al, and longer bonds increase along with the peak-shifts to longer atomic distance over the dose of 1.2×10^{23} e m^{-2}, indicating the development of medium- and long-range order of γ-Al_2O_3. On the other hand, the Al-O peak shows more complex behavior during irradiation, as shown in Fig. 6(b), where the Al-O

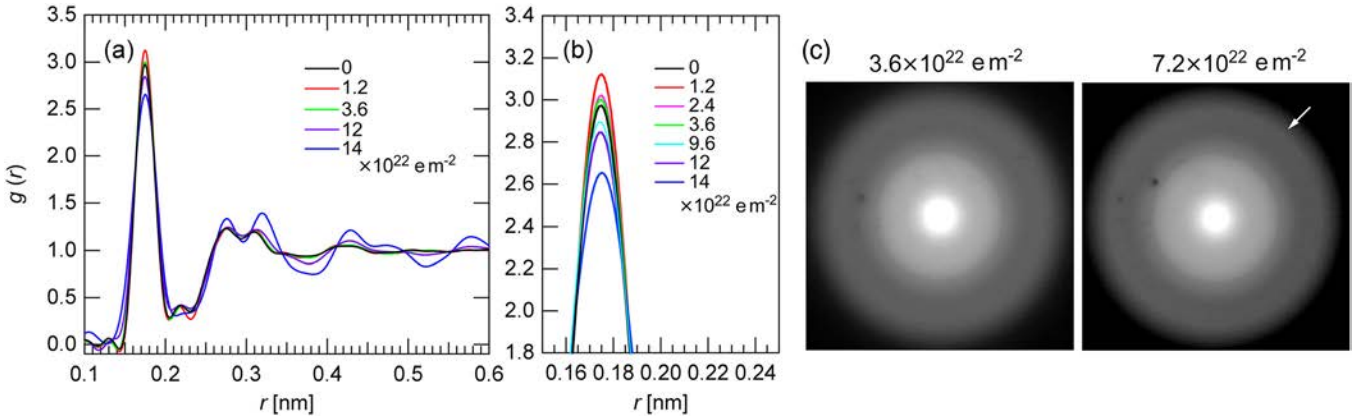

FIG. 6. (a) Changes in atomic pair distribution functions under irradiation at 100 keV with the dose rate of 4.0×10^{19} e $m^{-2}s^{-1}$ obtained by analyzing the SAED patterns taken from nearly identical regions of the specimen. (b) The enlarged part of the first peaks of (a) with the additional data. (c) The SAED pattern at the dose of 3.6×10^{22} e m^{-2}. The number density of atoms, ρ_0, is as follows: 89 nm^{-3} for 0 e m^{-2}, 90 nm^{-3} for 1.2×10^{22} e m^{-2}, 92 nm^{-3} for 2.4×10^{22} e m^{-2}, 96 nm^{-3} for 3.6×10^{22} e m^{-2}, 105 nm^{-3} for 9.6×10^{22} e m^{-2}, 110 nm^{-3} for 12.0×10^{22} e m^{-2}, and 120 nm^{-3} for 14.0×10^{22} e m^{-2}. The qualitative trend in ρ_0 is in agreement with the densification associated with crystallization.

peaks are enlarged along with the additional PDFs at two different conditions. Its peak intensity increases and then shows a maximum as indicated in the enlarged part of the peak at the early stage of irradiation (at the dose of 1.2×10^{22} e m^{-2}). It should be noted that the peak intensity turns into a decreasing trend after showing a maximum. Up to the dose of 3.6×10^{22} e m^{-2}, the peak intensity decreases without the appearance of Debye-Scherrer rings for γ-Al_2O_3 in the SAED patterns, as shown in Fig. 6(c). On the other hand, the further decrease of intensity over 9.6×10^{22} e m^{-2} takes place after the Debye-Scherrer ring for (440) plane appears at the dose of 7.2×10^{22} e m^{-2}, as indicated in Fig. 6(c).

It is known that PDFs are related to the number density of atoms, ρ_0 (for example, see formula (7) in Ref. 34). The ρ_0 can be estimated from the slope of the region below the first peak of the reduced radial distribution function,[36] and we confirmed that it gradually increases from 88 nm^{-3} to 120 nm^{-3} with irradiation (see the caption of Fig. 6). It is possible, therefore, to conclude that the decrease of the first peak over the dose of 9.6×10^{22} e m^{-2} is attributed to the densification by the appearance of γ-Al_2O_3. On the other hand, the peak intensity at the initial stage increases in spite of the slight density-increase of a-Al_2O_3, resulting from the structural change of a-Al_2O_3 itself. The PDFs have been previously analyzed for the annealed a-Al_2O_3 by *ex-situ* TEM observations, where neither systematic trend on the change in PDFs such as the decrease nor increase of the Al-O peak could be detected.[6,7] The difficulty in finding a systematic change in PDFs seems to arise mainly from the inhomogeneity of the thickness of samples, which were severally prepared for each annealing condition. On the contrary, the *in-situ* observation of a nearly identical region of irradiated a-Al_2O_3 gives a further advantage in capturing the sequential change in amorphous structure as mentioned above. In fact, a similar trend was obtained in the PDFs for the different irradiation energies of 75 and 300 keV. Therefore, the increase in Al-O peak intensity at the early stage of irradiation seems to reflect the structural change in amorphous Al_2O_3 before the crystallization, whereas the decrease in intensity results from the structural change towards the crystallization. The atomic density of γ-Al_2O_3 is much larger than that of amorphous Al_2O_3. If the amorphous phase directly crystallizes to the γ-phase, it is expected that the first peak due to Al-O monotonically decreases with crystallization. On the other hand, we found that the first Al-O peak increases at the initial stage of irradiation, suggesting that the stimulated state exists during the transformation from amorphous to γ-phase. In other words, the crystallization from the original amorphous state occurs via the excited and/or stimulated amorphous state.

The atomic-pair distribution functions of Fig. 6 are comprised of contributions from the original amorphous, stimulated amorphous, and γ-phase states. However, it is difficult to determine their volume fraction because of the inhomogeneous crystallization. The existence of the excited and/or stimulated amorphous state is consistent with the non-equilibrium thermodynamic system Qin *et al.* suggested.[37] According to them, the original amorphous phase with higher free energy goes to the crystalline phase with lower free energy under electron irradiation when the free-energy difference between them, namely, the released energy, is larger than the stored energy in the form of disordered atomic configuration. In general, the formation and migration of atoms in materials are enhanced by electron irradiation through electronic excitation and knock-on displacement processes.[38] Such an effect also helps the original amorphous state to reach to the stimulated state.

The transition processes of energy states from the original amorphous state to γ-Al_2O_3 under electron irradiation are illustrated in Fig. 7. What kinds of structural change at an atomic level occur at each stage shown in Fig. 7? The structure of amorphous Al_2O_3 is known to be composed of a majority of AlO_4 and AlO_5 basic units and some AlO_6 (original state in Fig. 7), while that of γ-Al_2O_3 is composed of AlO_4 and AlO_6 (the ratio of AlO_4/AlO_6 is 3/7-4/6).[2,6] The structural change from a-Al_2O_3 to γ-Al_2O_3 can be described by the change in ratio of AlO_4, AlO_5 and AlO_6 in terms of short-range order. It is believed that electronic excitation processes induce the breaking and rearrangement of thermodynamically less stable bonds in amorphous matrix.[32] In the

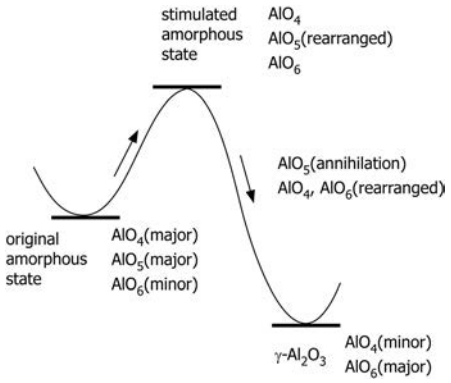

FIG. 7. The transition processes of energy states from the original amorphous state to γ-Al_2O_3 via the stimulated (excited) state in the irradiated region.

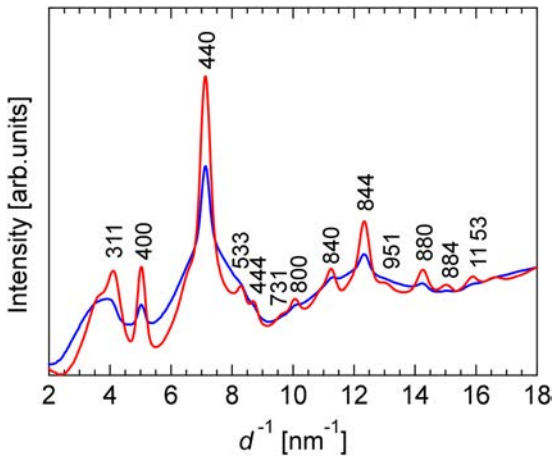

FIG. 8. The line profiles converted from the selected electron diffraction patterns of γ-Al_2O_3 irradiated for a long time at 100 keV. The blue and red lines correspond to the SAED patterns after the appearance of γ-Al_2O_3 from a-Al_2O_3 and a sufficiently long-time irradiation into γ-Al_2O_3, respectively.

case of a-Al_2O_3, the annihilation of unstable AlO_5 basic units is anticipated before the nucleation of γ-Al_2O_3. As mentioned by Lee *et al.*,[4] for example, the formation of edge sharing Al octahedrons from corner-sharing AlO_5 would occur in the transition stage from a-Al_2O_3 to γ-Al_2O_3. Therefore, one of the most probable reasons of the initial increase in peak intensity seems to be the breaking and rearrangement of AlO_5 basic units. On the other hand, the decrease in peak intensity and the broadening of Al-O bonds comes from the appearance of γ-Al_2O_3, that is, the decrease in AlO_4, the annihilation of AlO_5, and the increase in AlO_6. It is reasonable that the increase in AlO_6 with the longer bond-lengths and the decrease in AlO_4 with shorter bond-lengths cause the broadening of the first peak. Moreover, the decrease and broadening in Al-O peak are synchronized with the sharpening of the O-O, Al-Al, and longer bonds. The sharpening clearly indicates the development of medium- and long-range structures due to the crystallization. The *in-situ* observation and PDF analysis of electron-irradiation-induced crystallization of a-Al_2O_3 made it possible to reveal the structure of the excited (stimulated) amorphous Al_2O_3 appearing during the transition from the original amorphous to γ-Al_2O_3.

Finally, void formation mechanism in electron irradiated Al_2O_3 is discussed. Basically, the formation of nanovoids is attributed to the large density difference between a- and γ-Al_2O_3 on the macroscopic point of view. It is reasonable, therefore, that the void formation occurs as a result of crystallization of a-Al_2O_3 via not only annealing at high temperature around 1073 K (Refs. 5 and 7) but also electron-irradiation at ambient temperature. However, we found a difference in void formation behavior between annealed and irradiated γ-Al_2O_3: the void diameter in the irradiated γ-Al_2O_3 is smaller than in the annealed γ-Al_2O_3.The formation and growth of voids are accompanied by the crystal growth induced via long-range diffusion in the case of thermal annealing. On the other hand, a high density of nanocrystalline γ-Al_2O_3 with the diameter around 3 nm is formed via atomic displacement inside the irradiated region, thus resulting in the isolation of nanovoids in the restrictive area of nanocrystalline grains without the supply of free volume and the coalescence of voids. Although the grain growth of γ-Al_2O_3 occurs for a long-time irradiation as mentioned in Sec. III C, the effect of the grain growth on the growth of nanovoids is not so large.

C. Stability of γ-Al_2O_3 under electron irradiation

It is well-known that the types of structural change on ionic- and covalent-bonded crystalline materials induced by excitation-related mechanisms vary from material to material. In the case of amorphous SiO_2, for example, the structural change proceeds as amorphous SiO_2 → amorphous Si → crystalline Si by the electron irradiation with 200 keV, accompanied by the desorption of O_2 molecules;[25] the core-hole Auger decay process (K-F model)[39] is believed to operate for the decomposition of SiO_2. We observed the structural change of γ-Al_2O_3 for a long-time irradiation in order to understand the stability of a metastable γ-Al_2O_3 under lower electron-irradiation condition where the excitation mechanism operates preferentially as mentioned earlier. Figure 8 shows the changes in the line profiles of SAED patterns after the appearance of γ-Al_2O_3 from a-Al_2O_3 (blue line) and a sufficiently long-time irradiation into γ-Al_2O_3 (red line) under 100 keV. To enhance the oscillation at the large d^{-1} side (the high-angle side), the back-ground-subtracted intensity was multiplied by the scattering angle. All the Bragg reflections in both line profiles can be indexed consistently as the planes of γ-Al_2O_3 and their intensity increases with irradiation. We observed neither peaks of Al_2O_3 polytypes nor those for aluminum which is expected to form if K-F mechanism operates as is the case with amorphous SiO_2. Therefore, γ-Al_2O_3, which is composed of major AlO_6 and minor AlO_4, is stable against electronic excitation.

IV. CONCLUSION

The electron-beam-induced crystallization of a-Al_2O_3 was investigated by *in-situ* TEM under the wide incident electron-energy range of 25–300 keV. The conclusions of the present work were summarized as follows.

(1) The crystallization of a-Al_2O_3 into γ-Al_2O_3 is induced along with the formation of nanovoids in the crystalline phases by electron irradiation at 25–300 keV.

(2) The dose for crystallization decreases with irradiation energy, indicating that excitation-related processes dominantly operate in the crystallization of a-Al_2O_3.
(3) The structural change of a-Al_2O_3 emerges in the atomic pair distribution function as the increase in peak intensity of Al-O bonds around 0.18 nm, suggesting the breaking and rearrangement of short-range Al-O bonds. This rearranged structure corresponds to the excited and/or stimulated amorphous state before crystallization.
(4) As the crystallization of a-Al_2O_3 into γ-Al_2O_3 proceeds through electron-irradiation, the broadening of Al-O peak and the increase in peak intensity of O-O, Al-Al, and longer bonds become pronounced in the atomic pair distribution function: the former comes from the change in the ratio of basic units of $AlO_{4\text{-}6}$ and the latter indicates the development of long-period structure of γ-Al_2O_3.
(5) For a long-time electron irradiation, γ-Al_2O_3 transforms into neither Al_2O_3 polytypes nor aluminum precipitates, indicating that it is stable against electron irradiation.

ACKNOWLEDGMENTS

TEM observations using H-800 and H-7000 and JEM-3000F were performed at Research Center for Ultra-High Voltage Electron Microscopy (UHVEM) and Comprehensive Analysis Center of ISIR, Osaka University, respectively. The authors (R.N. and M.I.) are grateful to Mr. E. Taguchi for the technical support at UHVEM. This work was supported by Grant-in-Aid for Young Scientists (B) (No. 24760574).

[1]I. Levin and D. Brandon, J. Am. Ceram. Soc. **81**, 1995 (1998).
[2]G. Gutierrez and B. Johansson, Phys. Rev. B **65**, 104202 (2002).
[3]P. Vashishta, R. K. Kalia, A. Nakano, and J. P. Rino, J. Appl. Phys. **103**, 083504 (2008).
[4]S. K. Lee, S. B. Lee, S. Y. Park, Y. S. Yi, and C. W. Ahn, Phys. Rev. Lett. **103**, 095501 (2009).
[5]R. Nakamura, T. Shudo, A. Hirata, M. Ishimaru, and H. Nakajima, Scr. Mater. **64**, 197 (2011).
[6]M. Tane, S. Nakano, R. Nakamura, H. Ogi, M. Ishimaru, H. Kimizuka, and H. Nakajima, Acta Mater. **59**, 4631 (2011).
[7]R. Nakamura, M. Ishimaru, A. Hirata, K. Sato, M. Tane, H. Kimizuka, T. Shudo, T. J. Konno, and H. Nakajima, J. Appl. Phys. **110**, 064324 (2011).
[8]M. Digne, P. Sautet, P. Raybaud, P. Euzen, and H. Toulhoat, J. Catal. **226**, 54 (2004).
[9]D. G. Howitt and T. E. Mitchell, Philos. Mag. A **44**, 229 (1981).
[10]F. W. Clinard, Jr., G. F. Hurley, and L. W. Hobbs, J. Nucl. Mater. **108**, 655–670 (1982).
[11]A. Y. Stathopoulos and G. P. Pells, Philos. Mag. A **47**, 381 (1983).
[12]J. E. Bonevich and L. D. Marks, Ultramicroscopy **35**, 161 (1991).
[13]Y. Tomokiyo, T. Kuroiwa, and C. Kinoshita, Ultramicroscopy **39**, 213 (1991).
[14]G. P. Pells and T. Shikama, Philos. Mag. A **48**, 779 (1983).
[15]G. P. Pells and D. C. Phillips, J. Nucl. Mater. **80**, 207 (1979).
[16]G. P. Pells and D. C. Phillips, J. Nucl. Mater. **80**, 215 (1979).
[17]T. Shikama and G. P. Pells, Philos. Mag. A **47**, 369 (1983).
[18]S. H. Oh, Y. Kauffmann, C. Scheu, W. D. Kaplan, and M. Ruhle, Science **310**, 661 (2005).
[19]S. D. Berger, I. G. Salisbury, R. H. Milne, D. Imeson, and C. J. Humphreys, Philos. Mag. B **55**, 341 (1987).
[20]C. L. Chen, H. Furusho, and H. Mori, Philos. Mag. Lett. **90**, 715 (2010).
[21]C. L. Chen, K. Arakawa, and H. Mori, Scr. Mater. **63**, 355 (2010).
[22]C. L. Chen, K. Arakawa, J. G. Lee, and H. Mori, Scr. Mater. **63**, 1013 (2010).
[23]C. Pan, P. Shen, and S.-Y. Chen, J. Cryst. Growth **299**, 393 (2007).
[24]J. Murray, K. Song, W. Huebner, and M. O'Keefe, Mater. Lett. **74**, 12 (2012).
[25]M. Liu, L. Xu, and X. Lin, Scanning **16**, 1 (1994).
[26]X.-w. Du, M. Takeguchi, M. Tanaka, and K. Furuya, Appl. Phys. Lett. **82**, 1108 (2003).
[27]I. Stark, M. Stordeur, and F. Syrowatka, Thin Solid Films **226**, 185–190 (1993).
[28]L. Ba, Y. Qin, and Z. Wu, J. Appl. Phys. **80**, 6170 (1996).
[29]See supplementary material at http://dx.doi.org/10.1063/1.4790705 for in-situ observation of indium nanoparticles on an a-Al_2O_3 film (a) before and (b) after irradiation at 200 keV. The arrows in the BFIs indicate an identical indium nanoparticle before and after irradiation.
[30]E. Balanzat and S. Bouffard, Solid State Phenom. **30–31**, 7 (1992).
[31]S. J. Zinkle and C. Kinoshita, J. Nucl. Mater. **251**, 200 (1997).
[32]A. Meldrum, L. A. Boatner, and R. C. Ewing, J. Mater. Res. **12**, 1816 (1997).
[33]Y. Hirotsu, M. Ishimaru, T. Ohkubo, T. Hanada, and M. Sugiyama, J. Electron Microsc. **50**, 435 (2001).
[34]M. Ishimaru, Nucl. Instrum. Methods Phys. Res. B **250**, 309 (2006).
[35]P. Lamparter and R. Kniep, Physica B **234–236**, 405 (1997).
[36]For example, see S. R. Elliott, *Physics of Amorphous Materials*, 2nd ed. (Longman Scientific & Technical, 1990), p. 81.
[37]W. Qin, J. A. Szpunar, and Y. Umakoshi, Acta Mater. **59**, 2221 (2011).
[38]J. W. Corbett, *Electron Radiation Damage in Semiconductors and Metals* (Academic, New York, 1966).
[39]M. L. Knotek and P. J. Feibelman, Phys. Rev. Lett. **40**, 964 (1978).